Roll Modulation for Maximum Re-Entry Lateral Range

W. E. WAGNER*
Martin Company, Baltimore, Md.

Approximate solutions to the maximum re-entry lateral range problem are obtained for a maneuverable lifting re-entry vehicle performing coordinated maneuvers in pitch and roll. The solutions are obtained by several methods ranging from a simple multiphase decision process to a direct variational technique based on steepest descent. Numerical results are presented which demonstrate and compare the performance attained by means of the different methods. These results show the roll angle to increase with the nondimensional velocity. The percentage improvement in lateral range attained by modulating the roll angle rather than holding it constant at 45° increases with L/D. Furthermore, optimum roll modulation tends to reduce the amplitude of the phugoid skip.

Nomenclature

D = aerodynamic drag
g = acceleration of gravity at altitude
g_0 = acceleration of gravity at sea level
h = altitude
L = aerodynamic lift
l = lateral range
m = vehicle mass
P = penalty function
q = dynamic pressure
R = mean earth radius
r = distance from center of earth to vehicle
V = velocity
$\bar{V}$ = nondimensional velocity V/V_c
V_c = circular orbital velocity
x = state variables
X = longitudinal range
α = angle of attack
β = density exponent
γ = flight path angle
η = nondimensional velocity squared
λ = lagrange multipliers or adjoint variables
ρ = atmospheric density
ρ_0 = exponential density intercept
σ = roll angle about velocity vector
ϕ = roll angle about body axis
φ = lateral range angle
ψ = heading angle

Introduction

DURING re-entry of a satellite vehicle, the lateral range capability is of frequent concern, especially if landing or recovery is to occur at a specified ground location and "call down" from orbit is to be possible at frequent intervals. The problem of determining the vehicle's angle of attack and roll angle control functions, which yield maximum lateral range, requires variational techniques[1-3] for obtaining a solution. These methods use the principles of variational calculus to shape the control functions in a successive approximation manner utilizing the theory of steepest descent.

Because of the expense and difficulty involved in solving the lateral range problem by these variational methods, several approximate optimization techniques have been applied. In this paper, their results are compared with the more sophisticated methods. The various solutions are discussed individually and compared. The methods are presented in increasing degree of complexity, starting with a simple multiphase decision process in which the roll angle is approximated by n constant steps. Next the Eulerian boundary value problem is solved using simple approximate equations of motion. Finally, a direct variational technique based on steepest descent is presented which includes an elaborate re-entry mathematical model.

Presented as Preprint 64-471 at 1st AIAA Annual Meeting, Washington, D. C., June 29–July 2, 1964; revision received February 26, 1965.

* Senior Engineering Specialist, Aerospace Mechanics Department. Member AIAA.

Discussion

We begin by clearly stating the problem. Given a lifting re-entry vehicle that can perform coordinated maneuvers in pitch and roll, determine the roll angle and the angle-of-attack time histories that cause the vehicle to traverse a path through the atmosphere which terminates at a point that is displaced a maximum distance from the vertical plane containing the velocity vector at re-entry initiation.

Throughout the following discussion, reference is made to the roll angle σ measured about the velocity vector, rather than the more conventional roll angle ϕ measured about the longitudinal body axis. The two roll angles are easily related through the following equation:

$$\phi = \tan^{-1}\left[\frac{\sin\sigma}{\cos\alpha(\cos\sigma - \tan\gamma\,\tan\alpha)}\right] \quad (1)$$

where γ is the local flight path angle and α the angle of attack.

Earlier investigations have shown that, if the control functions are to be maintained at a constant level throughout the re-entry, a roll angle of approximately 45° and an angle of attack corresponding to $(L/D)_{max}$ yield maximum lateral range. One might suspect that the lateral range could be increased merely by increasing the roll angle so as to provide larger aerodynamic forces in the horizontal direction. This, however, reduces the vertical component of lift, causing the vehicle to descend to the denser portion of the atmosphere where re-entry is shortened because of the larger drag dissipation. To decrease the roll angle would cause the vehicle to re-enter at higher altitudes where smaller lateral forces are generated because of the smaller density. It appears evident from these two extremes that the correct roll angle should cause the vehicle to descend to such an altitude that the large dissipative drag forces are not excessive and yet the lateral forces generated are sufficient to accomplish the turning necessary to transfer the large kinetic energy to lateral range.

The various techniques used to determine the maximum lateral range are now discussed.

Method 1 Multiphase Roll Program

Probably the simplest method for determining the maximum lateral range is to approximate the continuous roll angle function by n constant steps. The optimum magnitude of each step as well as the $n - 1$ velocity separation

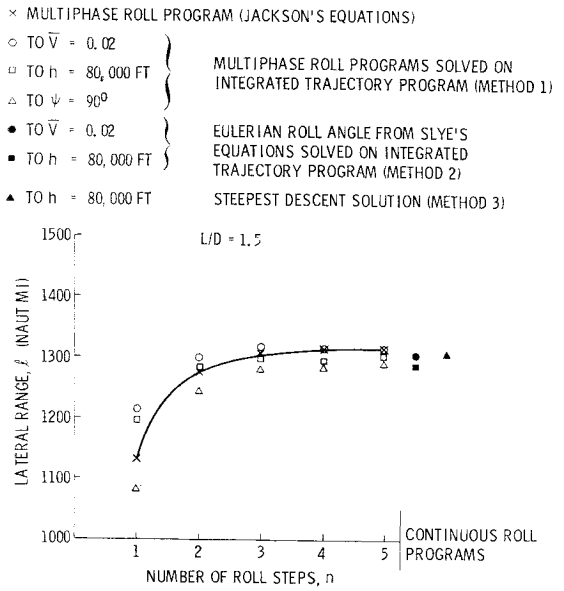

Fig. 1 Lateral range vs roll steps.

points is then solved by a successive approximation scheme based on steepest ascent in a $2n - 1$ dimensional Euclidean space. To expedite the computer solution, Jackson's difference equations for re-entry[4] are used as follows:

$$\psi_{n+1} = \psi_n + \frac{1}{2}\left[\left(\frac{L}{D}\right)\sin\sigma \ln\left(\frac{\eta_n}{\eta_{n+1}}\right) + \left(\frac{L}{D}\right)\cos\sigma \tan\varphi_n \cos\psi_n \ln\left(\frac{1-\eta_n}{1-\eta_{n+1}}\right)\right] \quad (2)$$

$$\varphi_{n+1} = \varphi_n + \frac{1}{2}\left(\frac{L}{D}\right)\cos\sigma\left[\frac{\sin\psi_n + \sin\psi_{n+1}}{2}\right] \times \ln\left(\frac{1-\eta_{n+1}}{1-\eta_n}\right) \quad (3)$$

where

$$\eta = \bar{V}^2 = V^2/gr \quad (4)$$

These equations assume that the component of gravity in the direction of the velocity vector is negligible, the path angle is small, and the time rate of change of the path angle is zero. Also assumed is that the roll angle and L/D are constant. Therefore, Eqs. (2) and (3) are solved repeatedly for each roll phase, during each of which the control functions are constant.

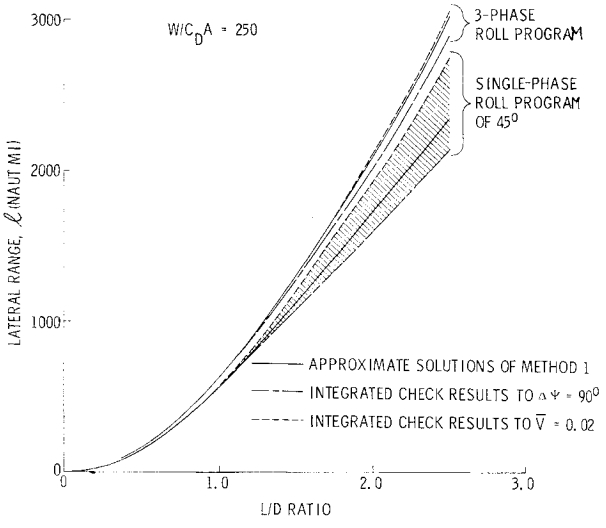

Fig. 2 Lateral range vs L/D ratio.

Initially estimating values for the roll angles to be used in each phase $\sigma_1, \sigma_2, \ldots, \sigma_n$ and the velocity separation points $\bar{V}_1, \bar{V}_2, \ldots, \bar{V}_{n-1}$, Eqs. (2) and (3) are solved from the initial conditions at $\bar{V}_0$ to final conditions at $\bar{V}_n$. The roll angles and velocity separation points are then updated by steepest ascent as follows:

$$\begin{aligned} \sigma_i^{k+1} &= \sigma_i^k + K(\partial\varphi_f/\partial\sigma_i) \qquad i = 1, 2, \ldots, n \\ \bar{V}_j^{k+1} &= \bar{V}_j^k + K(\partial\varphi_f/\partial\bar{V}_j) \qquad j = 1, 2, \ldots, n-1 \end{aligned} \quad (5)$$

where K is the step size. To first order, the total change in ϕ_f is

$$d\varphi_f = \sum_{i=1}^{n}\frac{\partial\varphi_f}{\partial\sigma_i}\Delta\sigma_i + \sum_{j=1}^{n-1}\frac{\partial\varphi_f}{\partial\bar{V}_j}\Delta\bar{V}_j \quad (6)$$

Since

$$\Delta\sigma_i = K(\partial\varphi_f/\partial\sigma_i) \text{ and } \Delta\bar{V}_j = K(\partial\varphi_f/\partial\bar{V}_j)$$

then

$$d\varphi_f = K\left[\sum_{i=1}^{n}\left(\frac{\partial\varphi_f}{\partial\sigma_i}\right)^2 + \sum_{j=1}^{n-1}\left(\frac{\partial\varphi_f}{\partial\bar{V}_j}\right)^2\right] \quad (7)$$

From Eq. (7), K can be determined for a specified change in ϕ_f. Knowing K, the updated values of σ and $\bar{V}$ are determined from Eq. (5). The process is repeated until no change in ϕ_f can be obtained. The partial derivatives in Eqs. (5–7) are obtained numerically.

Numerical results for the multiphase roll program technique are presented in Figs. 1–4 by the solid lines. Figure 1 shows lateral range vs number of roll steps for a vehicle having an L/D of 1.5. In Fig. 2 the lateral range is plotted as a function of L/D for 3-phase roll programs. Figure 3 relates roll angle to nondimensional velocity for 2-, 3-, 4-, and 5-phase roll programs, and Fig. 4 presents the 3-phase roll programs for different L/D ratios. Since Eqs. (2) and (3) only approximately determine the lateral range, the multiphase roll programs of Figs. 3 and 4 were checked on an accurate integrated re-entry program (spherical, nonrotating earth) for re-entry conditions given in Table 1. The resulting lateral ranges are shown in Figs. 1 and 2. The integrated trajectory results account for the zero roll terminal descent subsequent to attaining a heading angle change $\Delta\psi$ of 90°, whereas the approximate solutions execute a terminal spiral. The dark circles represent the lateral range achieved to a heading angle change of 90°, the shaded circles to an altitude of 80,000 ft, and the light circles to a nondimensional velocity of 0.02.

In Fig. 1, the lateral range is seen to increase significantly in going from a 1-phase to a 3-phase roll program. Above 3 phases little range, if any, is actually gained. Note that an increase in the lateral range to $\bar{V} = 0.02$ of 8.4% is obtained by increasing the number of roll phases from 1 to 3. Although the approximate equations [Eqs. (2) and (3)] yield the largest lateral range for a 5-phase roll program, the integrated check results show the 3-phase roll to be slightly better. This deviation is probably due to the assumptions involved in Eqs. (2) and (3).

In Fig. 2 lateral range vs L/D is given for an optimal 3-phase roll program and (for comparison) a single-phase roll program of 45°. Also shown are the integrated check results to a $\Delta\psi$ of 90° and to $\bar{V}$ of 0.02. From the check results to $\bar{V} = 0.02$, the increase in lateral range of the 3-phase from the 45° single-phase roll program is seen to be 8.4% at L/D of 1.5 and 10.7% at an L/D of 2.5. Thus the increase in optimal performance increases with L/D ratio.

Multiphase re-entries were generated with L/D also free to be optimized in each phase. In all cases, the L/D resulting was $(L/D)_{max}$. This might be expected from Eqs. (2) and (3), since if the lateral component of centrifugal force

(which is small) were neglected, the lateral range would be directly proportional to L/D.

Method 2 Eulerian Roll Angle Using Approximate Equations

The second method used for determining the roll angle function consists of formulating the problem as a Mayer problem of the calculus of variations. To simplify the analysis, Slye's approximate equations of motion[5] are used. These equations assume that the component of gravity in the direction of the velocity vector is negligible compared with drag, the path angle is small and its time rate of change is zero, and the lateral component of centrifugal force is negligible. The resulting first-order, nonlinear differential equations are

$$d\psi/d\bar{V} = -(L/D)(\sin\sigma/\bar{V}) \tag{8}$$

$$\frac{dl}{d\bar{V}} = \left(\frac{L}{D}\right)\frac{r\sin\psi\cos\sigma\bar{V}}{(\bar{V}^2-1)} \tag{9}$$

From the preceding equation it is seen that maximum lateral range occurs where L/D is maximum. The Euler-Lagrange equations corresponding to Eqs. (8) and (9) are

$$\frac{d\lambda_1}{d\bar{V}} = -\lambda_2\left(\frac{L}{D}\right)\frac{\bar{V}\cos\psi\cos\sigma r}{(\bar{V}^2-1)} \tag{10}$$

$$d\lambda_2/d\bar{V} = 0 \tag{11}$$

$$0 = \lambda_1\left(\frac{L}{D}\right)\frac{\cos\sigma}{\bar{V}} + \lambda_2\left(\frac{L}{D}\right)\frac{r\sin\psi\sin\sigma\bar{V}}{(\bar{V}^2-1)} \tag{12}$$

With initial conditions on ψ and l specified, the general transversality condition yields the following boundary conditions on the Lagrange multipliers at the terminal point:

$$\lambda_{2f} = -1 \tag{13}$$

$$\lambda_{1f} = 0 \tag{14}$$

Equations (11) and (13) yield $\lambda_2 = -1$ which, when substituted into (9), yields

$$\sigma = \tan^{-1}[\lambda_1(\bar{V}^2-1)/r\sin\psi\bar{V}^2] \tag{15}$$

and when substituted into Eq. (14) yields

$$\frac{d\lambda_1}{d\bar{V}} = \left(\frac{L}{D}\right)\frac{r\cos\psi\cos\sigma\bar{V}}{(\bar{V}^2-1)} \tag{16}$$

Equations (8, 9, 15, and 16), along with boundary conditions on l and ψ at the initial point and λ_1 from Eq. (14) at the terminal point, constitute the necessary relations that must be satisfied by the roll angle function for l to be maximum. These equations have been solved on an IBM 1620 computer, utilizing a simple trial-and-error process for determining the initial value of λ_1 required to give a solution that satisfied the terminal condition on λ_1.

The Eulerian roll angles for L/D of 0.2, 1.0, 1.8, and 2.5 are presented in Fig. 4, where they are compared with 3-phase roll programs. Figure 3 compares the 2-, 3-, 4-, and 5-phase roll programs with the Eulerian roll program for an L/D equal to 1.5. The Eulerian roll program appears to lie slightly below the multiphase roll programs in the velocity range from 0.4 to 0.9. This may be a result of neglecting the lateral component of centrifugal force in Eq. (8) upon which the Eulerian roll program is based. The Eulerian roll performance was also checked on an integrated trajectory program. The lateral range to $\bar{V} = 0.02$ which resulted is shown in Fig. 1 to be 0.92%, or 12 miles less than that for the 5-phase roll program.

Method 3 Steepest Descent Variational Solution

The steepest descent variational technique[3] was used next to solve the maximum lateral range problem. The re-entry

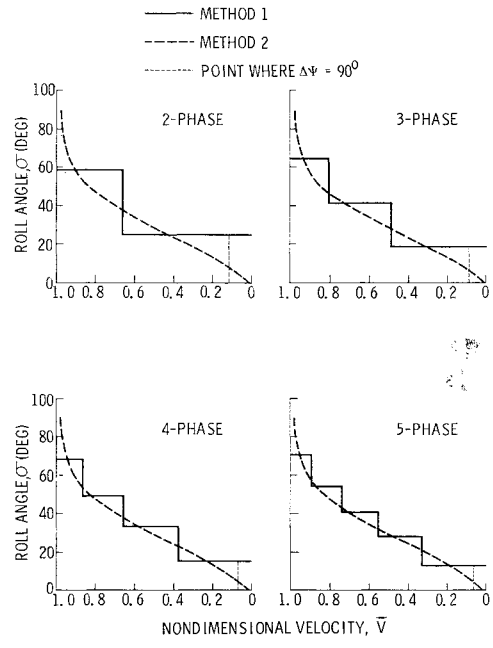

Fig. 3 Roll angle programs for $L/D = 1.5$.

equations used consist of the following:

$$\left.\begin{aligned}
\dot{V} &= -D/m - g\sin\gamma \\
\dot{\gamma} &= L\cos\sigma/mV + V\cos\gamma/(R+h) - g\cos\gamma/V \\
\dot{\psi} &= L\sin\sigma/mV\cos\gamma - V\cos\gamma\cos\psi\tan\varphi/(R+h) \\
\dot{h} &= V\sin\gamma \\
\dot{l} &= [R/(R+h)]V\sin\psi\cos\gamma \\
\dot{X} &= [R/(R+h)][V\cos\psi\cos\gamma/\cos(l/R)]
\end{aligned}\right\} \tag{17}$$

where

$$\left.\begin{aligned}
D &= C_D(\alpha)qS \qquad L = C_L(\alpha)qS \\
q &= \rho V^2/2 \qquad \rho = \rho_0 e^{-\beta h} \\
g &= g_0[R/(R+h)]^2
\end{aligned}\right\} \tag{18}$$

By initially estimating the control functions α and σ, Eqs.

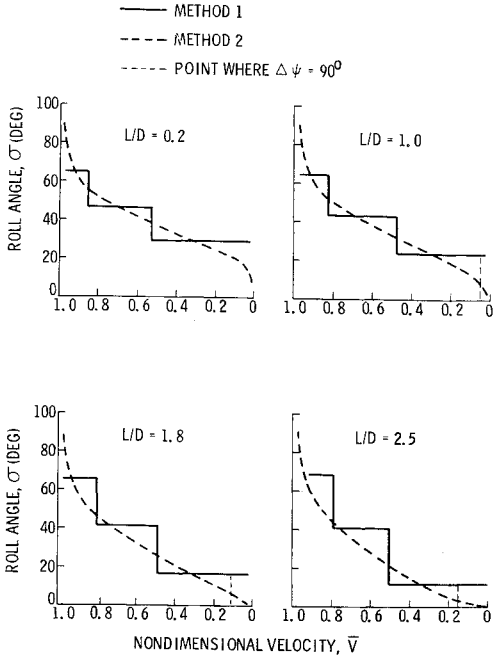

Fig. 4 Roll angle programs vs L/D.

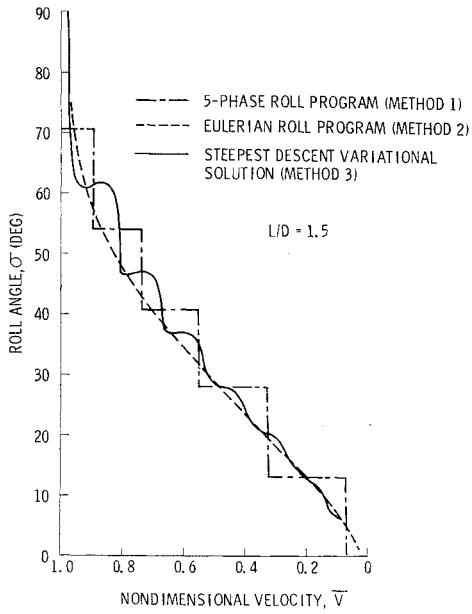

Fig. 5 Comparison of optimum roll angle programs.

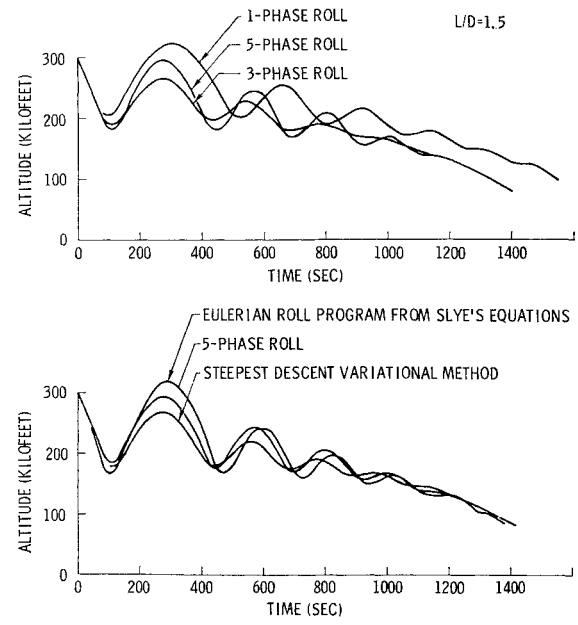

Fig. 7 Altitude vs time for various roll programs.

(17) can be solved from the known initial conditions of Table 1. Corrections to these control functions are then determined from solutions to a system of equations adjoint to perturbation equations about the nominal solution of Eqs. (17). These adjoint equations are solved backwards in time from initial conditions given by

$$\lambda_i(t_f) = (\partial P/\partial x_{i_{tf}}) - [\dot{P}(t_f)/\dot{h}(t_f)]$$

where P is the penalty function defined, for the maximum lateral range problem, to be $P = (l_{tf} - l^*)^2$, l^* being a number larger than the expected maximum lateral range. The successive approximation scheme has as its ultimate goal to minimize P (and thereby maximize the lateral range) by proceeding stepwise in the negative gradient (steepest descent) direction.

Numerical results were obtained on an IBM 7094 computer for a vehicle having an $L/D = 1.5$ and a $W/C_DA = 193$. The earth model was spherical nonrotating with the exponential atmosphere and initial conditions given in Table 1. The terminal altitude is 80,000 ft. The resulting optimal roll angle is presented in Fig. 5, where it is compared with the 5-phase roll program of method 1 and the Eulerian roll angle resulting from method 2. The maximum lateral range is presented in Fig. 1 where it is seen to be only 9 miles greater than the 5-phase roll program to 80,000 ft alt. The angle of attack that resulted from the optimization was essentially that for $(L/D)_{max}$.

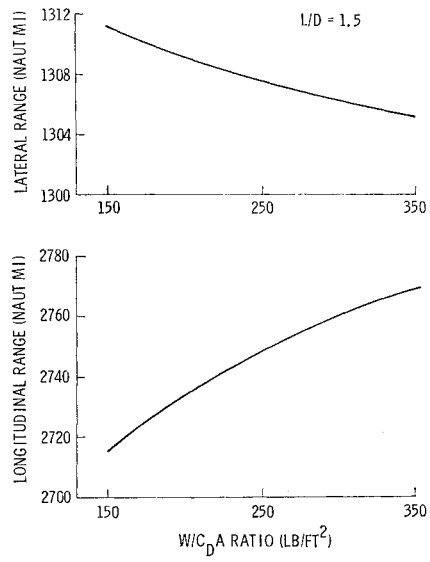

Fig. 6 Lateral and longitudinal range vs W/C_DA ratio

Results and Conclusions

Figures 1 and 2 indicate that very little lateral range capability is lost by approximating the optimum lateral range roll angle by a 3-phase roll program for vehicles having an L/D near 1.5. The percentage increase in the lateral range capability of a vehicle having optimum roll over that which results with a roll angle of 45° is proportional to the L/D ratio. For a vehicle having an L/D of 1.5, the maximum lateral range capability to 80,000 ft alt of a modulated roll angle program is approximately 9.5% greater than an optimum single-phase roll program.

The equations used in methods 1 and 2 show the maximum lateral range to be independent of W/C_DA. As an indication of the sensitivity of both lateral and longitudinal range on W/C_DA, Fig. 6 shows the lateral and longitudinal range as functions of W/C_DA for an $L/D = 1.5$ and the roll angle program of Fig. 4. As shown, the lateral range is very insensitive to W/C_DA, and the longitudinal range is only weakly dependent on the parameter.

Finally the effect of the various roll programs on re-entry shape is presented in Fig. 7. The first plot shows how the skip is reduced as the lateral range is increased. The second plot compares the approximate Eulerian program of method 2 and the steepest descent program of method 3. It appears as if the approximate Eulerian roll program of method 2 is farthest from optimum, conceivably as a result of neglecting the lateral component of centrifugal force in its determination. The 3-phase roll program compares very favorably with the steepest descent solution.

An item of practical concern which results from the study is the effort and expense involved in obtaining the last few

Table 1 Re-entry conditions for check trajectories

V_i	= 25,258.5 fps	h_i	= 300,000 ft
γ_i	= −3.0°	ψ_i	= 0
ρ	= $\rho_0 e^{-\beta \cdot h}$	ρ_0	= 0.0023769
g_0	= 32.256417 ft/sec²	β	= 4.25 × 10^{-5}
W	= 250 (method 1)		
C_DA	= 193 (methods 2 and 3)		

percentiles of capability. The multiphase roll programs appear to yield lateral ranges within several percent of the sophisticated steepest-descent solution, yet require only about $\frac{1}{50}$ the computation time and effort.

References

[1] Bryson, A. E., Mikami, K., and Battle, C. T., "Optimum lateral turns for a re-entry glider," Aerospace Eng. **21**, 18–23 (March 1962).

[2] Wagner, W. E., "Optimum trajectory program, UB-057 Part I—Program formulation," Martin Co., Space Systems Div., Rept. ER 12940 (April 1963).

[3] Wagner, W. E. and Jazwinski, A. H., "Three-dimensional re-entry optimization with inequality constraints," AIAA Preprint 63-419 (August 1963).

[4] Jackson, W. S., "An improved method for determining the lateral range of a gliding entry vehicle," J. Aerospace Sci. **28**, 910–911 (1961).

[5] Slye, R. D., "An analytical method for studying the lateral motion of atmospheric re-entry vehicles," NASA TN D-325 (September 1960).

SEPT.-OCT. 1965 J. SPACECRAFT VOL. 2, NO. 5

An Introduction to Gyro Optical Pickoffs

J. Richard Vyce*
Perkin-Elmer Corporation, Norwalk, Conn.

An optical pickoff provides a uniquely satisfactory solution to the problem of sensing the attitude of aerostatic, electrostatic, and cryomagnetic field-suspended spherical-rotor gyros that are invariably operated in the space-fixed mode. The servos in gimbaled gyros are controlled by the optical pickoff to maintain the pickoff aligned with the rotor, usually parallel to the rotor spin axis. Autocollimation permits true angle sensing uninfluenced by rotor translation, but an autocollimating pickoff requires a flat mirror on the rotor and normal to its spin axis. Alternatively, in cases where the rotor surface must be perfectly spherical, an autoreflector viewing a variable reflectivity pattern at a pole is used to sense polar translation, which is proportional to the angular misalignment of a center-fixed rotor. Field-suspended, strap-down gyros, that invariably employ spherical rotors, utilize an orthogonal set of autoreflecting pickoffs to sense the transit of a rotor surface pattern and a computer to determine the orientation of the spin axis from the pickoff signals. Autocollimator accuracy is shown to fall in the $\frac{1}{10}$ to 1 arc-sec region, whereas axial autoreflector accuracy is about 1 μin.; the strap-down readout system is capable of measuring with 10 to 100 arc-sec accuracy. Autocollimator and axial autoreflector accuracies are limited principally by the pickoffs themselves, whereas strap-down readout accuracy is restricted by the precision with which the sensing pattern can be applied to the rotor.

Introduction

ADVANCED gyro developments of recent years include a number of exotically levitated forms,[1] most of which introduce new and rather severe constraints to the problem of measuring rotor orientation. Briefly, the constraints arise from 1) the rotor isolation necessitated by the suspension system, 2) the inherent two-axis character of space-fixed gyros, 3) their exceedingly low-suspension torques, which made them highly susceptible to pickoff torques, and 4) the purely spherical rotors required in some configurations.

The most common gyro configuration involves a readout system usually consisting of angular position indicators on gimbal axes which is controlled to track the rotor by error signals from a null-sensing pickoff. The pickoff serves to indicate extremely minute rotor angular deviation from a fixed (null) relation to the pickoff, and, in view of the forementioned constraints, must 1) be extremely accurate, 2) indicate in two axes, 3) be capable of relatively remote operation, and 4) exert negligible torque and force at the rotor. An optical null-sensing pickoff, because of its accuracy, its remote operating capability, and its low reaction force, presently meets these requirements best and is, therefore, widely employed for exotic gyros. Two types are the autocollimator and the autoreflector. The former is generally preferable, but it requires that the rotor have a flat mirror surface normal to its spin axis. This feature can be accommodated by gas and cryomagnetic gyros, but the purely spherical rotor of the electrostatic gyro forces the use of an autoreflecting pickoff.

The relatively new strap-down gyro involves a space-fixed rotor whose attitude is measured by a set of direct-readout pickoffs that is at all times randomly related to it. Whereas the null-sensing pickoff indicates only small rotor misalignment, the direct-readout pickoff system must actually measure rotor attitude throughout its possible range of motion. The pickoffs themselves are autoreflectors that sense the transit of a line pattern on the rotor with extremely precise time resolution. A digital computer determines rotor orientation from the pickoff inputs. This strap-down, direct-readout system poses numerous problems for the pickoff and rotor pattern, as would be expected inasmuch as they essentially perform the combined function of the pickoff and gimbal-angle transducers on gimbaled gyros. (The strap-down gyro may be employed in place of a conventional gyro in any application and is not necessarily confined to a strap-down guidance system. Conversely, strap-down guidance systems may utilize conventional gyros. The strap-down designation simply indicates that certain functions formerly performed mechanically, such as rotor orientation measurement and accelerometer output resolution, are now done analytically.)

Presented as Preprint 63-314 at the AIAA Guidance and Control Conference, Massachusetts Institute of Technology, Cambridge, Mass., August 12–14, 1963; revision received April 15, 1965.

* Engineering Manager, Metrology; now Manager, Special Projects, Itek Corporation, Lexington, Mass.